Tribology International 72 (2014) 83–89

Contents lists available at ScienceDirect

Tribology International

journal homepage: www.elsevier.com/locate/triboint

The accuracy of the compressible Reynolds equation for predicting the local pressure in gas-lubricated textured parallel slider bearings

Mingfeng Qiu, Brian N. Bailey, Rob Stoll, Bart Raeymaekers *

Department of Mechanical Engineering, University of Utah, Salt Lake City, UT 84112, USA

ARTICLE INFO

Article history:
Received 2 September 2013
Received in revised form
30 November 2013
Accepted 9 December 2013
Available online 16 December 2013

Keywords:
Hydrodynamic lubrication
Surface texture
Reynolds equation

ABSTRACT

The validity of the compressible Reynolds equation to predict the local pressure in a gas-lubricated, textured parallel slider bearing is investigated. The local bearing pressure is numerically simulated using the Reynolds equation and the Navier–Stokes equations for different texture geometries and operating conditions. The respective results are compared and the simplifying assumptions inherent in the application of the Reynolds equation are quantitatively evaluated. The deviation between the local bearing pressure obtained with the Reynolds equation and the Navier–Stokes equations increases with increasing texture aspect ratio, because a significant cross-film pressure gradient and a large velocity gradient in the sliding direction develop in the lubricant film. Inertia is found to be negligible throughout this study.

1. Introduction

Surface texturing is used to enhance the load-carrying capacity of parallel slider bearings and to reduce friction and wear [1,2,3]. While groove-texture, and in particular spiral-grooved bearings [4] and herringbone-grooved bearings [5] have been used for several decades, surface microtexturing is a more recent development. Microtexture is commonly implemented as a dense array of micro-sized concave features ("dimples") fabricated using, e.g., laser surface texturing (LST) [6,7]. Reduced friction and increased load-carrying capacity have been reported for a spectrum of practical applications including journal bearings [8], thrust bearings [9,10], piston rings [11], mechanical seals [12,13], gas seals [14], and magnetic tape drive systems [15].

The local pressure distribution and the load-carrying capacity of a textured slider bearing are typically computed using the Reynolds equation. However, the presence of the surface texture potentially causes some of the key assumptions of the Reynolds equation to break down. Recently, a number of studies have discussed the validity of these assumptions to simulate hydrodynamic pressure in textured bearings with an incompressible lubricant, as a function of surface texture geometry and/or surface roughness and operating conditions [16–23]. Numerical solutions of the Navier–Stokes equations or Stokes equations are typically used to investigate the validity of the assumptions of the Reynolds equation. Hu and Leutheusser [16] studied parallel slider bearings with sinusoidal grooves on one of the bearing surfaces. For large Reynolds numbers they suggested that inertia is important when defining the limits of applicability of the Reynolds equation. Others have demonstrated that the Reynolds equation inaccurately predicts the pressure when the film thickness is on the same order of magnitude as the surface roughness feature wavelength (Stokes roughness) [17–19]. Arghir et al. [17] found that inertia becomes increasingly important when calculating the hydrodynamic pressure for a large Reynolds number flow. They concluded that this effect cannot be accurately simulated with the simplified Reynolds equation. In addition, van Odyck and Venner [18] demonstrated by comparing the solutions of the Stokes equations and the Reynolds equation that even without considering inertia, the results of the Reynolds equation display a significant difference with a more complete model for the case of Stokes roughness. Sahlin et al. [20] and Cupillard et al. [21] investigated inertia effects in infinitely long parallel sliders textured with two-dimensional dimples, by comparing results of the Navier–Stokes equations and the Stokes equations. The dimple depth and the film thickness were chosen to be on the same order of magnitude. Both studies confirm that inertia affects bearing load-carrying capacity. Similarly, de Kraker et al. [22] demonstrated that for simulating mixed lubrication in a textured bearing, the Reynolds equation with a cavitation model is appropriate when the film thickness is much smaller than the dimple depth. When the film thickness is larger than the dimple depth, inertia dominates and the Navier–Stokes equations must be used. Dobrica and Fillon [23] studied the effect of inertia as a function of the texture aspect ratio and concluded that the solutions of the Reynolds equation and the Navier–Stokes equations match well when the texture aspect ratio and the Reynolds

* Corresponding author. Tel.: +1 8015857594.
E-mail address: bart.raeymaekers@utah.edu (B. Raeymaekers).

0301-679X/$ - see front matter © 2013 Elsevier Ltd. All rights reserved.
http://dx.doi.org/10.1016/j.triboint.2013.12.008

Nomenclature

c	minimum spacing between the parallel bearing surfaces
c^*	reference minimum spacing, minimum spacing between bearing surfaces in the case of $\varepsilon=0.1$, $\delta=0.01$
$H(X,Y)$	non-dimensional local spacing $H(X,Y)=h(x,y)/c$
$h(x,y)$	local spacing between the bearing surfaces
h_p	dimple depth
L	total length of the textured bearing consisting of ten unit cells
$P(X,Y)$	non-dimensional local pressure, $P(X,Y)=p(x,y)/p_0$
$P^{NS}(X,Y)$	non-dimensional differential bearing pressure solution from the Navier–Stokes equations, $P^{NS}=(p^{NS}-p^{NS}_{avg})/p_0$
$P^{RE}(X,Y)$	non-dimensional differential bearing pressure solution from the Reynolds equation, $P^{RE}=(p^{RE}-p^{RE}_{avg})/p_0$
$\Delta P_r(X,Y)$	non-dimensional local pressure difference, $\Delta P_r=\|\|P^{RE}-P^{NS}\|\|_2/\|\|P^{NS}\|\|_2$
p	local pressure
p_0	atmospheric pressure
p_{avg}	average bearing pressure
$p^{NS}(x,y)$	local bearing pressure solution from the Navier-Stokes equations
$p^{RE}(x,y)$	local bearing pressure solution from the Reynolds equation
p^{NS}_{avg}	average bearing pressure from the Navier–Stokes equations
p^{RE}_{avg}	average bearing pressure from the Reynolds equation
R	velocity gradient ratio, $R=(\partial u/\partial x)/(\partial u/\partial z)$
R_{avg}	average velocity gradient ratio calculated for all finite volume cells
Re_{loc}	average local Reynolds number calculated for all finite volume cells
r_1	half-length of the square unit cell
r_p	dimple characteristic radius
S_p	texture density
U	relative sliding velocity
u	velocity in the x-direction
V	volume of the clearance between the bearing surfaces
V_l	volume of a tetrahedral cell l
v	velocity in the y-direction
$\mathbf{v}$	Velocity vector, $\mathbf{v}=[u, v, w]^T$
w	velocity in the z-direction
X,Y,Z	non-dimensional Cartesian coordinates, $X=x/r_p$, $Y=y/r_p$, $Z=z/c$
x,y,z	Cartesian coordinates
δ	non-dimensional minimum spacing between the bearing surfaces, $\delta=c/2r_p$
ε	texture aspect ratio, $\varepsilon=h_p/2r_p$
Λ	bearing number, $\Lambda=6\mu U r_p/(p_0c^2)$
Λ_m	modified bearing number, $\Lambda_m=6\mu UL/(p_0c^2)$
λ	flow parameter, $\lambda=3\mu U/2r_pp_0$
μ	gas dynamic viscosity
ρ	gas density

number are both small. For large values of the Reynolds number they found that the accuracy of the Reynolds equation can be improved significantly by introducing corrections for inertia. However, as pointed out by Feldman et al. [24], the conclusions of some of these studies must be interpreted with care because cavitation, which is the primary mechanism to generate load-carrying capacity in these bearings that use an incompressible lubricant, is either neglected [17–23] or treated in a simplified way [18].

Few studies document the validity and accuracy of the Reynolds equation to simulate bearings lubricated with a compressible fluid. Van Odyck and Venner [25] found that for a compressible parallel slider bearing with an asperity protruding from one surface, a large pressure gradient develops across the lubricant film thickness when increasing the relative sliding velocity between the bearing surfaces. Nevertheless, they concluded that the load-carrying capacity is predicted accurately by the Reynolds equation. Asperity texture on a parallel slider bearing with elastohydrodynamic lubrication was studied by Almqvist and Larsson [26]. They found that the Reynolds equation inaccurately predicts the local bearing pressure when the ratio of the film thickness and the horizontal asperity feature wavelength is larger than 0.01. This is a similar conclusion to the results shown in [17–19]. Additionally, Guardino et al. [27] studied sinusoidal roughness on a Rayleigh step bearing, and concluded that the Reynolds equation accurately predicts the load-carrying capacity when the roughness is small in amplitude compared to the film thickness. The only study to directly evaluate the validity of the Reynolds equation for gas-lubricated textured bearings was performed by Feldman et al. [24]. They evaluated a hydrostatic bearing, i.e., pressure driven flow, and concluded that the load-carrying capacity of the bearing is predicted accurately by the Reynolds equation despite some of the simplifying assumptions being violated locally for certain operating conditions.

Most of these studies focus on validating the prediction of the load-carrying capacity by the Reynolds equation as a function of the texture geometry. Hence, the validity of the Reynolds equation to predict load-carrying capacity in textured bearings is well established for both incompressible and compressible fluids. However, the breakdown of the assumptions inherent to the Reynolds equation when simulating textured bearings with a compressible lubricant has only been partially addressed. In addition to applications where it is sufficient to predict the load-carrying capacity, an accurate prediction of local pressure is the first step in developing fast and accurate particle and mass transport simulations, and is essential in lubricant–solid interaction problems for the case of elastohydrodynamic lubrication and foil bearings [28]. Moreover, no published studies exist that evaluate the validity of the Reynolds equation for modeling shear driven lubricant flow in gas-lubricated, textured slider bearings. Therefore, the objective of this paper is to evaluate the validity and accuracy of the compressible Reynolds equation for gas-lubricated textured parallel slider bearings. We compare simulation results of the Navier–Stokes equations and Reynolds equation, specifically focusing on computing the local bearing pressure and evaluating the accuracy of the assumptions inherent in the application of the Reynolds equation.

2. Methodology

2.1. Model description

Fig. 1 shows a gas-lubricated textured parallel slider bearing. Fig. 1(a) displays the x–z cross-section along the center line of the dimple and Fig. 1(b) shows the top view of the bearing. The dimple is a segment of a sphere of radius r_p and depth h_p, and is centered

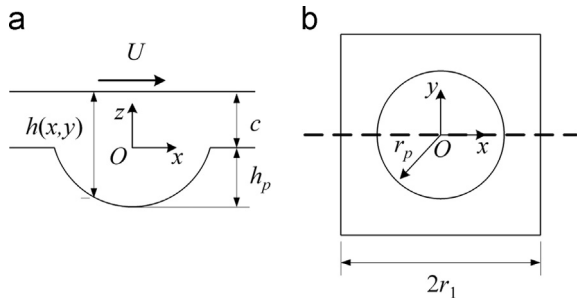

Fig. 1. Textured parallel slider bearing with one dimple: (a) x–z cross-sectional view; (b) top view (z-direction).

in a square unit cell of length $2r_1$. The local spacing between the bearing surfaces is denoted by $h(x,y)$.

A model for the bearing pressure between the two sliding surfaces is developed using the following assumptions: (1) the lubricant is air in laminar flow; (2) the relative sliding velocity U is constant, and much smaller than the speed of sound in the lubricant. Therefore, the gas flow is isothermal, isoviscous and the density is directly proportional to pressure (ideal gas); (3) hydrodynamic lubrication is maintained; (4) the bearing spacing is much larger than the mean free path of the gas. Thus, no slip occurs between the gas and any of the solid walls. Under these assumptions the following steady-state mass and momentum conservation equations describe the three-dimensional flow field in the bearing (compressible Navier–Stokes (NS) equations),

$$\nabla\cdot(\rho\mathbf{v})=0$$

$$\rho\mathbf{v}\cdot\nabla\mathbf{v}=-\nabla p+\mu\nabla^2\mathbf{v}+\frac{1}{3}\mu\nabla(\nabla\cdot\mathbf{v}), \tag{1}$$

where ρ is the density of air, $\mathbf{v}=[u,\ v,\ w]^{\mathrm{T}}$ is the velocity vector with components corresponding to velocity in the x-, y- and z-directions (Fig. 1). p is the local pressure and μ is the dynamic viscosity. The energy equation and the viscosity constitutive equation are not needed because constant temperature and viscosity are maintained. Periodic boundary conditions are enforced at the inlet and outlet of the dimple cell to account for the patterned texture in the stream-wise direction, while symmetric boundary conditions are applied on the lateral boundaries of the cell to model the presence of adjacent dimples in the span-wise direction. Thus,

$$\mathbf{v}|_{x=-r_1}=\mathbf{v}|_{x=r_1},\quad p|_{x=-r_1}=p|_{x=r_1}$$

$$v|_{y=-r_1}=v|_{y=r_1}=0,\quad \left.\frac{\partial u}{\partial y}\right|_{y=-r_1}=\left.\frac{\partial u}{\partial y}\right|_{y=r_1}=0,\quad \left.\frac{\partial v}{\partial y}\right|_{y=-r_1}=\left.\frac{\partial v}{\partial y}\right|_{y=r_1}=0$$

$$\left.\frac{\partial w}{\partial y}\right|_{y=-r_1}=\left.\frac{\partial w}{\partial y}\right|_{y=r_1}=0,\quad \left.\frac{\partial p}{\partial y}\right|_{y=-r_1}=\left.\frac{\partial p}{\partial y}\right|_{y=r_1}=0$$

$$\mathbf{v}|_{z=c}=[U,0,0]^{\mathrm{T}},\quad \mathbf{v}|_{z=c-h(x,y)}=\mathbf{0}. \tag{2}$$

Three key assumptions are made to derive the Reynolds equation from the Navier–Stokes equations (Eq. (1)) [28]; (1) the pressure is constant across the lubricant film thickness because the vertical dimension (z-direction) is much smaller than the other dimensions (x- and y-directions); (2) the dominant spatial velocity gradient is $\partial u/\partial z$; and (3) inertia effects are neglected because of the small sliding velocity and extremely small bearing spacing [15,24]. Hence, the steady-state two-dimensional (2D) compressible Reynolds equation (RE) in non-dimensional form is given as

$$\frac{\partial}{\partial X}\left(PH^3\frac{\partial P}{\partial X}\right)+\frac{\partial}{\partial Y}\left(PH^3\frac{\partial P}{\partial Y}\right)=\frac{\lambda}{\delta^2}\frac{\partial(PH)}{\partial X}, \tag{3}$$

where $X=x/r_p$ and $Y=y/r_p$ are the non-dimensional Cartesian coordinates, and r_p is the dimple radius. The non-dimensional local pressure $P(X,Y)=p(x,y)/p_0$ is the local air bearing pressure divided by the atmospheric pressure p_0. The non-dimensional local spacing $H(X,Y)=h(x,y)/c$ is the local spacing divided by the minimum spacing between the bearing surfaces c. $\lambda=3\mu U/2r_p p_0$ is the flow factor and $\delta=c/2r_p$ is the non-dimensional minimum spacing between the sliding surfaces. λ and δ describe the operating conditions of the textured bearing. The texture aspect ratio ε is defined as the ratio of the dimple depth over the diameter, $\varepsilon=h_p/2r_p$. Similar to Eq. (2), the boundary conditions for the RE are periodic in the stream-wise direction, and symmetric on the lateral boundaries.

2.2. Numerical simulation

The following dimensional parameters are used to solve the NS equations. The dynamic viscosity of air at room temperature $\mu=1.8\times10^{-5}$ Pa s. The relative sliding velocity between the bearing surfaces $U=10$ m/s. The dimple radius $r_p=50$ μm, typical for engineering applications [14,24,29]. The effect of the texture radius, when the texture aspect ratio remains constant, is minimal. The texture density $S_p=0.15$, which is favorable in terms of maximizing hydrodynamic bearing pressure [30]. To fully explore the effect of texture geometry across a wide range of values used in experiments [23], the dimple depth is varied between 5.0 and 50.0 μm so that the dimple geometry ranges from very shallow to a hemisphere. The minimum spacing between the bearing surfaces, c, is varied between 0.3 and 2.0 μm, relevant to different applications [15,29]. Table 1 summarizes the bearing operating and design parameters studied in this paper, displayed in non-dimensional form. 56 combinations of texture aspect ratio and bearing spacing are investigated. The so-called "Stokes roughness" (ratio of film thickness to texture characteristic length in the x-direction) [17,18] does not fall within the range of operating conditions considered in this study and, thus, its influence on the validity of the Reynolds equation is not investigated.

The NS equations are solved using a commercial finite volume computational fluid dynamics software package (FLUENT version 6.3.26). A non-conformal mesh is used to discretize the computational domain. The upper (rectangular) channel uses a uniform hexahedral mesh, while the dimple is discretized using tetrahedral elements. The meshing is challenging in particular for shallow dimple geometries and small bearing spacing. Element sizes are chosen to suit the geometry of each case such that further refinement does not change the average bearing pressure by more than 0.01%. The geometries examined in this study use numerical grids ranging from 1.1×10^6 discrete volumes in the case of the largest dimple depth to 6.3×10^6 volumes in the case of the smallest dimple depth and smallest bearing spacing. Smaller dimple depths required very small grid volumes in order to have enough volumes in the vertical direction. When combined with volume aspect ratio limits, a large number of volumes is required to fill the horizontal extent of the dimple. The resulting execution times are approximately 3–24 h per case including meshing time.

The RE is solved iteratively by discretizing Eq. (3) using a second order central finite difference scheme on a 251-by-251 staggered grid [31]. Convergence of the non-dimensional pressure solution is assumed to occur when the relative change in pressure at every grid node is less than 10^{-5} between two successive iterations. The computing time for each case is typically less than

Table 1
Textured bearing parameters investigated in this study.

Flow factor, λ	Texture density, S_p	Texture aspect ratio, ε	Non-dimensional spacing, δ
5.3×10^{-5}	0.15	0.010–0.500	0.003–0.020

one minute on a similar computer than the one used for the NS simulations. The pressure results computed using the RE ($p^{RE}(x,y)$) are compared with the NS solution for pressure at the upper sliding surface ($p^{NS}(x,y)$) (Fig. 1), and the assumptions of the RE are quantitatively evaluated using the NS solution. All the results are presented as a function of the non-dimensional quantities ε and δ, which are key parameters for determining bearing performance [12].

Compressible flow simulations with periodic boundary conditions in FLUENT require a reference pressure at a fixed point in the solution domain to solve Eq. (1). The arbitrary treatment of this reference point precludes direct comparison of absolute pressure values needed to determine the load-carrying capacity. However, it does not affect the ability to compare local bearing pressure results. The average pressure computed for both the NS (P^{NS}_{avg}) and RE (P^{RE}_{avg}) simulations is subtracted from the respective absolute local pressure results, and both are non-dimensionalized with the atmospheric pressure p_0. Finally, the non-dimensional results of the pressure simulations obtained with the NS equation $P^{NS} = (p^{NS} - p^{NS}_{avg})/p_0$ and with the RE $P^{RE} = (p^{RE} - p^{RE}_{avg})/p_0$ are compared.

3. Results and discussion

3.1. Local bearing pressure

The non-dimensional local pressure difference ΔP_r between the RE and NS solutions is defined as the vector norm (L_2-norm [32]) of the difference between both non-dimensional pressure solutions, divided by the vector norm of the non-dimensional NS pressure solution.

$$\Delta P_r = \frac{\|P^{RE} - P^{NS}\|_2}{\|P^{NS}\|_2}, \tag{4}$$

Fig. 2 shows ΔP_r contour lines as a function of the texture aspect ratio ε and the non-dimensional bearing spacing δ. It is observed that the deviation of the local pressure between the RE and NS solutions is almost independent of δ, but increases with ε. The RE predicts the local pressure accurately for most of the texture geometries, as suggested by $\Delta P_r \leq 0.03$ for $\varepsilon \leq 0.05$, which is especially important in modeling and optimizing texture geometry for gas-lubricated bearings [30]. However, ΔP_r increases to approximately 0.2 for $\varepsilon = 0.25$, and becomes larger than 0.7 when ε approaches 0.5 (hemispherical dimple geometry).

Fig. 3 displays the local non-dimensional differential pressure, P^{RE} and P^{NS}, along the center line of the top bearing surface for the

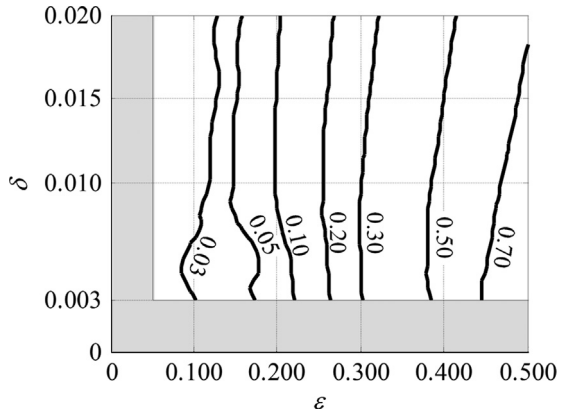

Fig. 2. Non-dimensional local pressure difference ΔP_r between the RE and the NS solutions calculated using the L_2 norm. The gray-shaded area limits the range of the non-dimensional bearing spacing and texture aspect ratio evaluated.

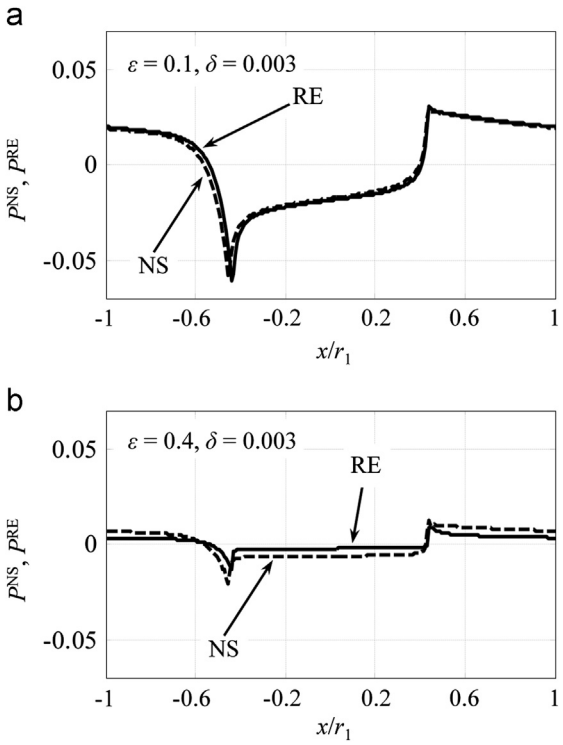

Fig. 3. Local non-dimensional differential pressure along the center line of the upper surface of the textured bearing obtained with the RE (P^{RE}) and NS (P^{NS}) equations for (a) $\varepsilon = 0.1$, $\delta = 0.003$; (b) $\varepsilon = 0.4$, $\delta = 0.003$.

case of (a) $\varepsilon = 0.1$, and (b) $\varepsilon = 0.4$ with $\delta = 0.003$. These results illustrate that solutions obtained with the RE and the NS equations match well for small texture aspect ratios (e.g., less than 10% relative difference for $\varepsilon = 0.1$). However, a large deviation may occur for large ε values (e.g., approximately 50% relative difference for $\varepsilon = 0.4$).

3.2. Cross-film pressure gradient

The RE assumes that because of the extremely small vertical dimension of the bearing (z-direction) compared to the other two horizontal dimensions (x- and y-directions), the pressure remains constant across the lubricant film thickness. This assumption can be evaluated by examining the curvature of the isobar contour lines computed from the NS solution along the x–z cross-section through the center line of the textured bearing. Fig. 4 shows the isobar contour lines for four different combinations of texture aspect ratio ε and non-dimensional spacing δ. To scale the vertical bearing dimension uniformly for the four cases, the local spacing $h(x,y)$ is non-dimensionalized with the minimum bearing spacing c of the dimple in Fig. 4(a), which will be referred to as c^*.

For both small (Fig. 4(a) and (c)) and large (Fig. 4(b) and (d)) values of the texture aspect ratio ε, the isobar contour lines are almost independent of the non-dimensional minimum spacing δ. This indicates that the effect of δ on the cross-film pressure gradient is negligible. Additionally, for a small value of ε the isobars remain mostly perpendicular to the primary flow direction (x-direction) across the lubricant film thickness both inside and outside the dimple area (Fig. 4(a) and (c)). For a large ε value, the isobar contours are no longer perpendicular to the x-direction across the lubricant film thickness in the entire dimple geometry. In particular, close to the bottom surface and the inlet/outlet of the dimple (Fig. 4(b) and (d)), the isobars display significant curvature. This indicates that the pressure is no longer constant across the lubricant film thickness. Thus, the cross-film

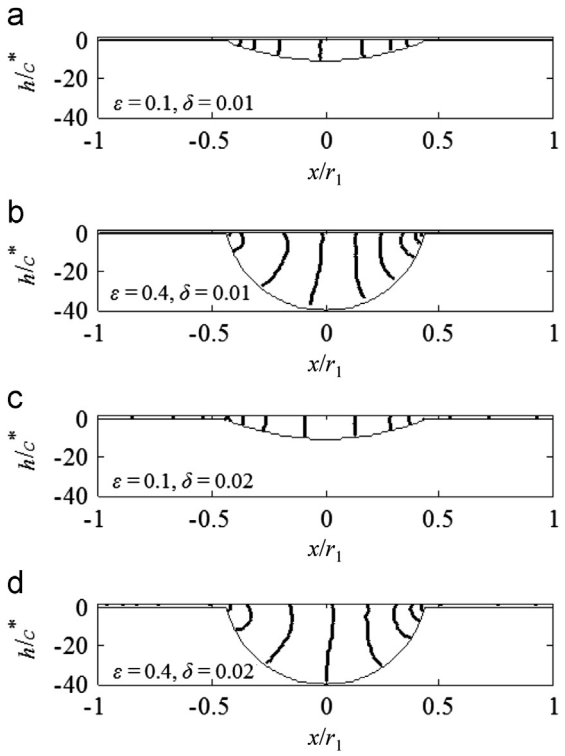

Fig. 4. Isobar contour lines in the x–z cross-section along the center line of the textured bearing: (a) ε=0.1, δ=0.01; (b) ε=0.4, δ=0.01; (c) ε=0.1, δ=0.02; (d) ε=0.4, δ=0.02. To scale all sub-figures uniformly, the vertical dimension is normalized with the minimum spacing c^* in the case of (a).

pressure gradient is negligible for small values of ε, but becomes more significant with increasing ε. Note that compared to pressure-driven flow in textured bearings, the cross-film gradient in shear-driven flow is much less significant [24].

3.3. Velocity gradients

The RE assumes that the only dominant spatial gradient of the velocity components is the derivative of u with respect to the z-direction (Fig. 1), which means that the ratio $R=(\partial u/\partial x)/(\partial u/\partial z)$ is assumed to approach zero. The volume between the sliding bearing surfaces is triangulated into tetrahedral cells using the nodes of the finite volume elements from the NS solution. R is calculated at the center of each tetrahedral cell, and is then averaged over the total volume to yield R_{avg},

$$R_{avg} = \frac{1}{V}\sum_l \left(\left| \frac{\partial u}{\partial x} \Big/ \frac{\partial u}{\partial z} \right|_l V_l \right), \tag{5}$$

where V_l is the volume of each tetrahedral cell l, and V is the total volume between the bearing surfaces. Fig. 5 displays R_{avg} contour lines as a function of the texture aspect ratio ε and non-dimensional spacing δ.

From Fig. 5 it is observed that R_{avg} is almost independent of δ, but increases with increasing ε. R_{avg} reaches approximately 0.2 when ε is larger than 0.25 and exceeds 0.5 for ε approaching 0.5. This indicates that the two velocity gradients $(\partial u/\partial x)$ and $(\partial u/\partial z)$ are approaching the same order of magnitude. Thus, the assumption of negligible velocity gradient with respect to the x-direction is violated for dimples with a large texture aspect ratio, which correlates well with the deviation in the local pressure calculation (Fig. 2).

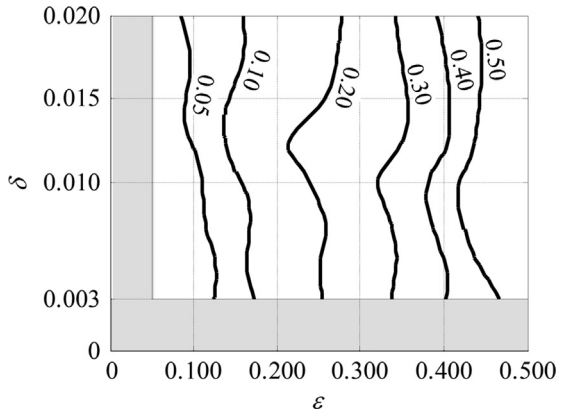

Fig. 5. Average ratio of velocity gradients in the x- and z-directions R_{avg} as a function of ε and δ. The gray-shaded area limits the range of the non-dimensional bearing spacing and texture aspect ratio evaluated.

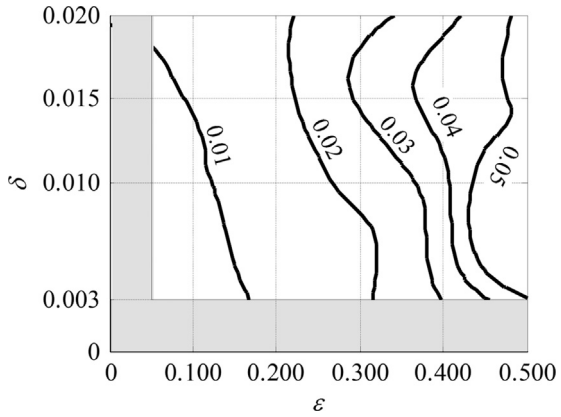

Fig. 6. Average local Reynolds number as a function of ε and δ. The gray-shaded area limits the range of the non-dimensional bearing spacing and texture density evaluated.

3.4. Local inertia effects

The inertia effects in the flow field are examined by computing the local ratio of inertia forces and viscous forces in the NS solution. This local Reynolds number is estimated at the center of each tetrahedral cell (as discussed in Section 3.3) from the NS solution [33], and averaged throughout the total volume of the bearing spacing (Eq. (6)). The definitions of V_l and V are the same as in Eq. (5). Fig. 6 displays the result for different combinations of texture aspect ratio ε and non-dimensional spacing δ.

$$\mathrm{Re}_{loc} = \frac{1}{V}\sum_l \left(\left| \frac{\rho \mathbf{v} \nabla u}{\mu \nabla^2 u + \frac{1}{3}\mu \frac{\partial}{\partial x}(\nabla \mathbf{v})} \right|_l V_l \right), \tag{6}$$

Fig. 6 shows that the cell-averaged local Reynolds number is smaller than 0.05 for almost any combination of ε and δ, which indicates that inertia is indeed negligible compared to viscosity in the bearing spacing throughout the range of parameters considered. Note that the local Reynolds number increases with increasing texture aspect ratio ε, indicating that the effect of inertia becomes more important as the dimple depth increases.

3.5. Recirculation flow

Several authors have attempted to describe the effect of recirculation flow in textured bearings. Sahlin et al. [20] and Cupillard et al. [21] both emphasized that vortices have an influence on the bearing load-carrying capacity. Feldman et al.

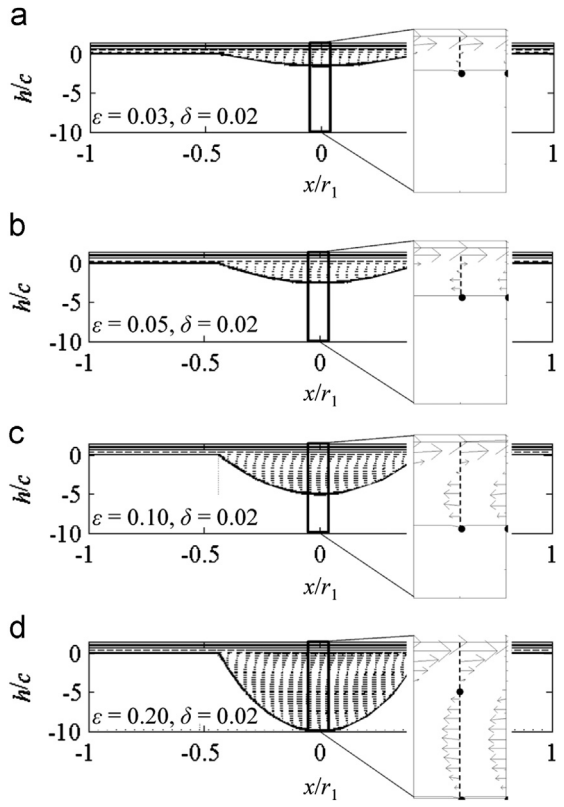

Fig. 7. Velocity vectors for the *x*-*z* cross-section along the center line of the textured bearing, δ=0.02; (a) ε=0.03; (b) ε=0.05; (c) ε=0.1; (d) ε=0.2. The insets show a magnification of the velocity profile at the deepest point of the dimple.

[24] also suggested that the inception of recirculation flow affects the validity of the Reynolds equation in predicting pressure for hydrostatic gas bearings. In this study, recirculation is evaluated by examining the NS velocity profiles in the *x*–*z* cross-section along the center line of the textured bearing. Fig. 7 displays four dimples with different texture aspect ratios and equal non-dimensional minimum spacing δ. When the texture aspect ratio is small (ε=0.03, Fig. 7 (a)) the stream-wise velocity stays positive or near zero everywhere, suggesting no recirculation. With increasing texture aspect ratios, a recirculation zone forms in the dimple, clearly indicated by the negative stream-wise flow velocity in the lower region of the dimple. The recirculation region increases with increasing texture aspect ratio, and the stream-wise velocity becomes more negative (Fig. 7(b–d)). As also pointed out in [24], the development of recirculation regions indicates a large gradient of velocity with respect to the *x*-direction, violating the assumption of negligible stream-wise velocity gradient inherent in the RE. This is illustrated by the increase of recirculation with increasing texture aspect ratio in Fig. 7 and Fig. 5.

3.6. Discussion

For small ε and δ, the RE and NS solutions of the local bearing pressure show minimal deviation. These texture geometries are also the most difficult ones for which to create a high quality mesh required for the NS solution. The maximum bearing spacing is several orders of magnitude smaller than the bearing length and width and, thus, a very large number of finite volume cells are needed to resolve this geometry, which also requires significant computing time. In contrast, for these geometries the RE performs exceptionally well in terms of both accuracy and computational cost.

The deviation between the NS and RE solutions for the local bearing pressure increases with increasing ε. This deviation can largely be explained by the breakdown of the assumption that the dominant velocity gradient is $\partial u/\partial z$. The ratio of the velocity gradients in the flow direction and the vertical direction increases with increasing texture aspect ratio ε, which matches the increasing deviation between the local pressure computed with the RE and NS equations (Fig. 2 and Fig. 5). The development of recirculation flow is found to be associated with increasing inaccuracy of the local pressure prediction by the RE compared to the NS equations, which can also be attributed to significant velocity gradients in the *x*-direction. The development of a cross-film pressure gradient also contributes to the inaccuracy in the local pressure prediction (Fig. 4). The reason for the breakdown of these two assumptions with increasing texture aspect ratio is likely that with increasing ε the vertical and horizontal dimensions of the dimple become similar. Thus, the assumption of a significantly smaller vertical bearing dimension ceases to be accurate.

The non-dimensional parameters used in this study are particularly relevant to textured bearings. Conventional notation uses the bearing number Λ to describe compressibility effects. In this study, for a single dimple the bearing number can be expressed as $\Lambda=\lambda/\delta^2=6\mu U r_p/(p_0 c^2)$. To compare with traditional gas bearings a modified bearing number $\Lambda_m=6\mu UL/(p_0 c^2)$ can be defined using a characteristic length equal to the total length of the bearing L. Assuming a bearing with 10 unit cells (L is approximately 2.3 mm), Λ_m ranges from 6 to 270 for the range of ε and δ values used in this study. This suggests that compressibility effects are important in this type of textured bearings and that a compressible flow model has to be used in this study.

4. Conclusion

The validity and accuracy of the compressible Reynolds equation in predicting the local pressure in a gas-lubricated, textured parallel slider bearing is studied by comparing the local bearing pressure obtained with the Reynolds equation and the Navier–Stokes equations for a single dimple textured bearing model. The following conclusions are made.

(1) Deviation between the local pressure obtained with the Reynolds equation and the Navier–Stokes equations exists. This deviation is independent of the bearing spacing but increases with increasing texture aspect ratio. Beyond a texture aspect ratio of ε=0.25, the deviation of the local pressure between the two models may exceed 20%.
(2) The deviation between the local pressure solution of the Reynolds equation and the Navier–Stokes equations for increasing texture aspect ratio can be explained by the breakdown of the assumption that the stream-wise velocity vertical gradient dominates the other velocity gradients and by the development of a significant cross-film pressure gradient.
(3) Inertia effects are confirmed to be negligible for the range of bearing and texture parameters considered in this study.

References

[1] Kovalchenko A, Ajayi O, Erdemir A, Fenske G, Etsion I. The effect of laser surface texturing on transitions in lubrication regimes during unidirectional sliding contact. Tribol Int 2005;38:219–25.
[2] Wang X, Adachi K, Otsuka K, Kato K. Optimization of the surface texture for silicon carbide sliding in water. Appl Surf Sci 2006;253:1282–6.
[3] Galda L, Pawlus P, Sep J. Dimple shape and distribution effect on characteristics of Stribeck curve. Tribol Int 2009;42:1505–12.
[4] Malanoski SB. Pan CHT. The static and dynamic characteristics of the spiral-grooved thrust bearing. J Basic Eng-T, 87. ASME; 1965; 547–55.

[5] Vohr JH, Chow CY. Characteristics of herringbone-grooved, gas-lubricated journal bearings. J Basic Eng-T ASME 1965;87:568–76.
[6] Etsion I. State of the art in laser surface texturing. J Tribol-T ASME 2005;127:248–53.
[7] Vilhena LM, Sedlacek M, Podgornik B, Vizintin J, Babnik A, Mozina J. Surface texturing by pulsed Nd:YAG laser. Tribol Int 2009;42:1496–504.
[8] Lu X, Khonsari MM. An experimental investigation of dimple effect on the stribeck curve of journal bearings. Tribol Lett 2007;27:169–76.
[9] Wang X, Kato K, Adachi K, Aizawa K. Loads carrying capacity map for the surface texture design of SiC thrust bearing sliding in water. Tribol Int 2003;36:189–97.
[10] Etsion I, Halperin G, Brizmer V, Kligerman Y. Experimental investigation of laser surface textured parallel thrust bearings. Tribol Lett 2004;17:295–300.
[11] Ronen A, Etsion I, Kligerman Y. Friction-reducing surface-texturing in reciprocating automotive components. Tribol T 2001;44:359–66.
[12] Etsion I, Kligerman Y, Halperin G. Analytical and experimental investigation of laser-textured mechanical seal faces. Tribol T 1999;42:511–6.
[13] Yu XQ, He S, Cai RL. Frictional characteristics of mechanical seals with a laser-textured seal face. J Mater Process Tech 2002;129:463–6.
[14] McNickle AD, Etsion I. Near-contact laser surface textured dry gas seal. J Tribol-T ASME 2004;126:788–94.
[15] Raeymaekers B, Etsion I, Talke FE. Enhancing tribological performance of the magnetic tape/guide interface by laser surface texturing. Tribol Lett 2007;27:89–95.
[16] Hu J, Leutheusser HJ. Micro-inertia effects in laminar thin-film flow past a sinusoidal boundary. J Tribol-T ASME 1997;119:211–6.
[17] Arghir M, Roucou N, Helene M, Frene J. Theoretical analysis of the incompressible laminar flow in a macro-roughness cell. J Tribol-T ASME 2003;125:309–18.
[18] van Odyck DEA, Venner CH. Stokes flow in thin films. J Tribol-T ASME 2003;125:121–32.
[19] Song DJ, Seo DK, Schultz WW. A comparison study between Navier–Stokes equation and Reynolds equation in lubricating flow regime. KSME Int J 2003;17:599–605.
[20] Sahlin F, Glavatskih SB, Almqvist T, Larsson R. Two-dimensional CFD-analysis of micro-patterned surfaces in hydrodynamic lubrication. J Tribol-T ASME 2005;127:96–102.
[21] Cupillard S, Glavatskih SB, Cervantes MJ. Inertia effects in textured hydrodynamic contacts. P I Mech Eng J-J Eng 2010;224:751–6.
[22] de Kraker A, van Ostayen RAJ, van Beek A, Rixen DJ. A multiscale method modeling surface texture effects. J Tribol-T ASME 2007;129:221–30.
[23] Dobrica MB, Fillon M. About the validity of Reynolds equation and inertia effects in textured sliders of infinite width. P I Mech Eng J-J Eng 2009;223:69–78.
[24] Feldman Y, Kligerman Y, Etsion I, Haber S. The validity of the Reynolds equation in modeling hydrostatic effects in gas lubricated textured parallel surfaces. J Tribol-T ASME 2006;128:345–50.
[25] van Odyck DEA, Venner CH. Compressible stokes flow in thin films. J Tribol-T ASME 2003;125:543–51.
[26] Almqvist T, Larsson R. Some remarks on the validity of Reynolds equation in the modeling of lubricant film flows on the surface roughness scale. J Tribol-T ASME 2004;126:703–10.
[27] Guardino C, Chew JW, Hills NJ. Calculation of surface roughness effects on air-riding seals. J Eng Gas Turb Power 2004;126:75–82.
[28] Hamrock BJ, Schmid SR, Jacobson BO. Fundamentals of fluid film lubrication. 2nd ed.. New York: Marcel Dekker Inc; 2004.
[29] Kligerman Y, Etsion I. Analysis of the hydrodynamic effects in a surface textured circumferential gas seal. Tribol T 2001;44:472–8.
[30] Qiu M, Delic A, Raeymaekers B. The effect of texture shape on the load-carrying capacity of gas-lubricated parallel slider bearings. Tribol Lett 2012;48: 315-327.
[31] Lacey CA, Talke FE. A tightly coupled numerical foil bearing solution. IEEE T Magn 1999;26:3039–43.
[32] Bronshtein IN, Semendyayev KA, Musiol G, Muehlig. H. Handbook of Mathematics. 5th ed.. Berlin; New York: Springer; 2007.
[33] Correa CD, Hero R, Ma K. A comparison of gradient estimation methods for volume rendering on unstructured meshes. IEEE T Vis Comput Gr 2011;17:305–19.